Journal of Controlled Release 377 (2025) 93–105

Contents lists available at ScienceDirect

Journal of Controlled Release

journal homepage: www.elsevier.com/locate/jconrel

Nanotherapeutics-mediated restoration of pancreatic homeostasis and intestinal barrier for the treatment of severe acute pancreatitis

Juanhui Lin [a,1], Yuansong Wei [b,1], Xiaxian Gu [a], Miaoru Liu [a], Mengru Wang [a], Renxiang Zhou [b], Duowu Zou [c], Lichen Yin [b,*], Chunhua Zhou [c,*], Duanmin Hu [a,*]

[a] Department of Gastroenterology, The Second Affiliated Hospital of Soochow University, Suzhou 215004, China
[b] Institute of Functional Nano and Soft Materials (FUNSOM), Jiangsu Key Laboratory of Carbon-Based Functional Materials and Devices, Soochow University, Suzhou 215123, China
[c] Department of Gastroenterology, Ruijin Hosptial, Shanghai Jiao Tong University School of Medicine, Shanghai 200025, China

ARTICLE INFO

Keywords:
Severe acute pancreatitis
Intestinal barrier dysfunction
Anti-oxidant
Anti-inflammation
Interleukin 22
Nanotherapeutics

ABSTRACT

Severe acute pancreatitis (SAP) is an inflammatory disease of the pancreas accompanied with intestinal injury, and effective therapeutic modalities are still highly lacking. Herein, a facile and effective nanotherapeutics (pHA@IBNCs) is developed to alleviate pancreatic inflammation and restore intestinal barrier for SAP treatment. Epigallocatechin gallate (EGCG, an anti-oxidant), interleukin-22 (IL-22, an anti-inflammatory and epithelial barrier-protecting cytokine), and bovine serum albumin (a framework protein), are assembled *via* non-covalent interactions to form nanocomplexes (IBNCs). Then, phenylboronic acid-modified hyaluronic acid (pHA) is synthesized and coated onto IBNCs *via* formation of the reversible boronate ester bonds to obtain pHA@IBNCs. Upon intravenous injection, pHA@IBNCs could efficiently accumulate at the lesion sites of sodium taurocholate (STC)-induced SAP mice, based on their prolonged blood circulation time and pHA-mediated targeting of activated intestinal epithelial cells and macrophages. Inside the inflammatory microenvironment, over-produced reactive oxygen species (ROS) trigger the shedding of the pHA layer and release of the drug payloads. Thereby, EGCG cooperates with IL-22 to attenuate pancreatitis and restore the intestinal barrier by scavenging ROS, suppressing pro-inflammatory cytokines secretion, and promoting the repair of intestinal epithelia. Such a nano-therapeutic approach targeting multiple pathological events may serve as a promising paradigm for the effective management of SAP.

1. Introduction

Severe acute pancreatitis (SAP) is one of the most critical diseases in the clinical setting, with an overall mortality rate of up to 30 % [1,2]. The primary cause of death is multiple organ failure resulting from systemic inflammatory response syndrome or infection-induced sepsis [3–5]. Current clinical treatment of SAP is still limited to fluid management and supportive care [6–8]. Thus, the development of effective pharmaceutics/therapeutics for SAP management is of utmost importance.

Accumulating evidences have unraveled that intestinal dysfunction and systemic inflammation secondary to local inflammation in the pancreas work together to aggravate SAP retroactively. During the early stage of SAP, injured acinar cells secrete pro-inflammatory cytokines and chemokines to recruit and activate macrophages and neutrophils, creating a localized inflammatory environment in the pancreas [9,10]. Excessive inflammatory response leads to edema in the pancreatic, peripancreatic, and retroperitoneal tissues, and the massive extravasation of tissue fluids finally results in hypoxia and ischemia/reperfusion (I/R) in other organs. Intestinal tissue is most susceptible to SAP-induced I/R [11]. During the ischemia stage, the accumulation of succinate and reduced production of adenosine 5′-triphosphate (ATP) lead to impaired mitochondrial function. Following reperfusion, the accumulated succinate is rapidly re-oxidized by succinate dehydrogenase, driving the extensive generation of reactive oxygen species (ROS) *via* reverse electron transport at the mitochondrial complex I. Overproduced ROS in the intestinal tract then decrease the expression of tight junction-associated proteins (such as ZO-1 and Occludin) and cause the apoptosis of

* Corresponding authors.
E-mail addresses: lcyin@suda.edu.cn (L. Yin), zhou_chunh@163.com (C. Zhou), huduanmin@163.com (D. Hu).
[1] Juanhui Lin and Yuansong Wei contributed equally.

https://doi.org/10.1016/j.jconrel.2024.11.022
Received 12 August 2024; Received in revised form 3 October 2024; Accepted 10 November 2024
Available online 17 November 2024

intestinal epithelial cells (IECs) [12–16]. As a consequence, the intestinal barrier is disrupted, allowing bacteria to invade the blood to aggravate systemic inflammatory responses. At the meantime, ROS decrease the number of intestinal stem cells (ISCs), which hurdle the restoration of intestinal barrier by inhibiting the epithelial regeneration in the damaged area. Therefore, a therapeutic strategy that can concurrently scavenge ROS, suppress pro-inflammatory cytokine secretion, and restore intestinal barrier is highly imperative for the treatment of SAP.

Epigallocatechin gallate (EGCG), a natural product with strong ROS-scavenging and anti-oxidant capacities, has revealed promising potential for the treatment of inflammatory diseases, such as hepatic injury, sepsis, and ulcerative colitis [17–24]. On the other hand, interleukin-22 (IL-22) is known to exert a multifaceted protective effect on the intestinal barrier by inhibiting the production of pro-inflammatory cytokines, along with its ability to foster the proliferation of ISCs *via* the IL-22/STAT3 axis [25–28]. Based on the complementary functions of EGCG and IL-22 in anti-oxidation, anti-inflammation, and intestinal protection, we reason that co-administration of EGCG and IL-22 may represent an enlightened approach for SAP management with robust efficacy. However, upon systemic administration, free EGCG or IL-22 suffers from short circulation half-life and rapid clearance, resulting in inefficient accumulation to the inflamed site. Fortunately, EGCG could form nanocomplexes (NCs) with proteins through non-covalent interactions such as hydrogen bonding, π-π stacking, hydrophobic interaction, *etc.*, thus allowing nano-assembly of the co-delivered EGCG and IL-22 to improve their pharmacokinetics profiles [29]. Nevertheless, the undesired serum tolerance and lack of targeting ability of these delivery systems still pose challenges against the effective *in vivo* utilization.

Herein, inflammation-targeted, IL-22/EGCG co-delivered nanotherapeutics was developed to mediate effective SAP management by concurrently scavenging ROS, inhibiting inflammation, and restoring intestinal barrier. For *in vivo* application, the dose of EGCG used is often 100–1000-fold higher than IL-22. Whereas, EGCG forms stable NCs with proteins normally at the EGCG/protein weight ratios of 0.1–3 [30–32]. As thus, bovine serum albumin (BSA), a non-immunogenic and non-toxic natural protein, was introduced as a framework component to assist the co-assembly with EGCG and IL-22, thereby forming stable and uniform NCs (IBNCs). Phenylboronic acid-modified hyaluronic acid (pHA) was then designed and decorated onto the surface of IBNCs through the reversible boronate ester bonds, which created a protective shell that enhanced the serum stability of NCs and reduced the drug

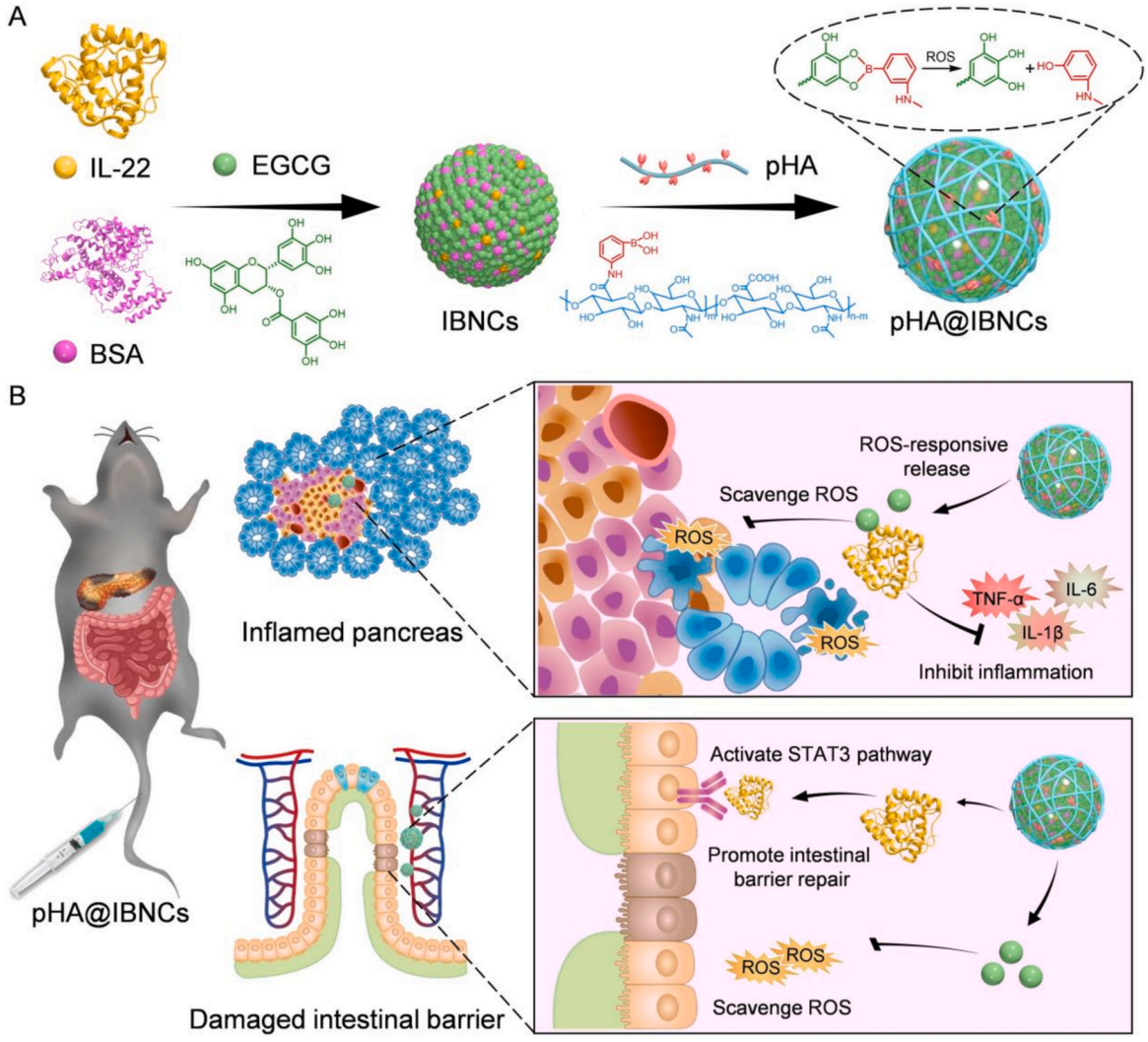

Scheme 1. Illustration of inflammation-targeted, IL-22/EGCG co-delivered, and ROS-responsive pHA@IBNCs for the management of SAP. (A) Preparation of pHA@IBNCs. (B) *In vivo* performance of pHA@IBNCs. In sodium taurocholate (STC)-induced SAP mice, intravenously injected pHA@IBNCs efficiently accumulated at the inflamed pancreas and colon due to pHA-mediated active targeting of CD44, wherein the over-produced H_2O_2 disrupted the boronate ester bonds to shed off the pHA shell and promote the drug release. IL-22 and EGCG then cooperated to alleviate the oxidative stress, inhibit inflammation, and restore the intestinal barrier.

leakage during blood circulation [33–35]. Moreover, pHA coating facilitated the accumulation of NCs to the lesion sites of sodium taurocholate (STC)-induced SAP mice, mainly *via* recognition of overexpressed CD44 on the surfaces of IECs in the inflamed intestine and activated macrophages in the inflamed pancreas and intestine [36,37]. Within the inflammatory microenvironment, the boronate ester bonds could be cleaved by H_2O_2, resulting in the consumption of ROS and H_2O_2-responsive pHA shedding [35,38–42]. The exposed IBNCs then dissociated to release IL-22 and EGCG in the H_2O_2-enriched inflammatory microenvironment, thereby allowing IL-22 and EGCG to cooperatively alleviate oxidative stress, inhibit inflammation, promote intestinal barrier repair, and restore pancreatic homeostasis in sodium taurocholate (STC)-induced SAP mice (Scheme 1).

2. Materials and methods

2.1. Materials, animals, and cells

EGCG, potassium persulfate, and 2,2′-azino-bis(3-ethylbenzthiazoline-6-sulfonic acid) (ABTS) were purchased from Macklin (Shanghai, China). 1,1-Diphenyl-2-picrylhydrazyl (DPPH), collagenase I, collagenase IV, alizarin red S (ARS), and Hank's balanced salt solution (HBSS) were purchased from Solarbio (Beijing, China). 3-Aminobenzeneboronic acid (ABA) was purchased from Adamas (Shanghai, China). Hyaluronic acid (HA, 40 kDa) was purchased from Bloomage Freda Biopharm (Shandong, China). Recombinant murine IL-22 was purchased from Peprotech (Rocky Hill, NJ, USA). BSA was purchased from Biosharp (Anhui, China). Ethylenediaminetetraacetic acid (EDTA) was purchased from Aladdin (Shanghai, China). *N*-(3-dimethylaminopropyl)-*N*′-ethylcarbodiimide hydrochloride (EDC), *N*-hydroxysuccinimide (NHS), STC, methylene blue, fluorescein isothiocyanate-labeled dextran (FITC-dextran, 4 kDa), lipopolysaccharide (LPS, from *Escherichia coli* 0111:B4), and *N*-(2-hydroxyethyl)piperazine-*N*′-2-ethanesulfonic acid (HEPES) were purchased from Sigma-Aldrich (St. Louis, MO, USA). Myeloperoxidase (MPO) assay kit and amylase assay kit were purchased from Nanjing Jiancheng (Nanjing, China). Cyanine5-NHS (Cy5-NHS), Cy3-NHS, and Cy5-labeled HA (^{Cy5}HA) were purchased from Qiyue Biology (Xi'an, China). Dihydroethidium (DHE) and H_2O_2 assay kit were purchased from Beyotime (Shanghai, China). TNF-α, IL-6, IL-1β, and IL-22 ELISA kits were purchased from Invitrogen (Carlsbad, US). All antibodies for immunoblot and immunofluorescence analyses were purchased from Abcam (Cambridge, Britain), Immunoway (Newark, USA), or Cell Signaling Technology (Massachusetts, USA). PrimeScript RT kit and SYBR Premix Ex Taq kit were purchased from Takara (Beijing, China). Primers were purchased from GenePharma (Shanghai, China), and their sequences were shown in Table S1.

Male C57BL/6 mice (8–10 weeks) were obtained from Shanghai Slaccas Experimental Animal Co., Ltd. (Shanghai, China) and housed in a specific pathogen-free (SPF) room, four to a cage, with access to food and water *ad libitum*, a 12:12 h light-dark cycle (8:00–20:00), and a temperature of 25 ± 1 °C. All the animal experiments were approved by the Institutional Animal Care and Use Committee at Soochow University. The animal experimental protocols were performed in accordance with the NIH guidelines for the care and use of laboratory animals (NIH Publication No. 85–23 Rev. 1985).

Primary mouse intestinal epithelial cells (MIECs) were isolated as described previously [43]. Briefly, the intestinal tissue (10 mg) was harvested from healthy mice, opened longitudinally, rinsed with HBSS to remove fecal contents, cut into 2–4-mm pieces, incubated with digestion solution (10 mM EDTA and 200 U collagenase IV/mL in 5 mL PBS) for 2 h, and washed with HBSS for three times. After filtering through nylon mesh (200 mesh) and centrifugation at 1500 rpm for 5 min, the cell pellet was resuspended and cultured in Dulbecco's Modified Eagles Medium (DMEM) containing 10 % fetal bovine serum (FBS). Primary mouse pancreatic acinar cells (MPACs) were isolated as described previously [44]. Briefly, the pancreas tissue (10 mg) was harvested from healthy mice, cut into 2–4-mm pieces, digested with fresh digestion solution (10 mM HEPES, 200 U collagenase I/mL, and 0.25 mg trypsin inhibitor/mL in 5 mL HBSS) for 2 h at 37 °C. After filtering through nylon mesh (200 mesh) and centrifugation at 1500 rpm for 5 min, the cell pellet was resuspended and cultured in DMEM containing 10 % FBS. RAW 264.7 cells were purchased from the American Type Culture Collection (Rockville, MD, USA), and cultured in DMEM containing 10 % FBS.

2.2. Synthesis of pHA

HA (400 mg, 1.05 mmol of -COOH group) was dissolved in deionized (DI) water (50 mL), into which EDC (776 mg, 5 mmol) and NHS (575 mg, 5 mmol) were added. After stirring for 1 h, ABA solution (6.8 mg/mL in ethanol, 20 mL) was added dropwise and stirred at room temperature for 24 h. The resulting solution was dialyzed against DI water (MWCO = 3.5 kDa) and lyophilized to obtain pHA. ^{1}H nuclear magnetic resonance (^{1}H NMR) spectrum of pHA dissolved in DMSO-d_6/D_2O (1/1, *v/v*) was recorded on a Varian ^{UNITY}INOVA-400 spectrometer. Chemical shifts (δ) were reported in the units of ppm and referenced to the protonic impurities. Cy5-labeled pHA (^{Cy5}pHA) was synthesized from ^{Cy5}HA and ABA using the similar procedure as described above.

2.3. Synthesis of fluorescence-labeled proteins

Briefly, Cy5-NHS solution (4 mg/mL in DMSO, 10 μL) was added to IL-22 solution (0.5 mg/mL in 0.1 M $NaHCO_3$ solution, 1 mL). The mixture was stirred at room temperature for 12 h in the dark, dialyzed against DI water (MWCO = 3.5 kDa) for 2 d, and lyophilized to yield ^{Cy5}IL-22. Cy3- and Cy5-labeled BSA were similarly prepared.

2.4. Preparation and characterization of pHA-coated BSA/EGCG nanocomplexes (pHA@BNCs)

pHA@BNCs were prepared *via* two sequential self-assembly steps in the aqueous solution: (1) complexation between BSA and EGCG to produce the inner core; (2) surface-coating with pHA *via* formation of boronate ester bonds. Particularly, EGCG (0.05, 0.15, 0.35, 0.5, or 0.7 mg/mL in DI water, 1 mL) and BSA (4 mg/mL in DI water, 250 μL) were mixed and stirred at 37 °C for 30 min to form the EGCG/BSA NCs (BNCs). The product was purified *via* ultrafiltration (MWCO = 100 kDa) to remove the un-encapsulated EGCG or BSA. pHA solution (1.25 or 2.5 mg/mL in DI water, 1 mL) was then added. The mixture was stirred at room temperature for 30 min and purified by ultrafiltration (MWCO = 100 kDa) to form pHA@BNCs. The obtained BNCs and pHA@BNCs were characterized for hydrodynamic size and zeta potential using the Malvern Zetasizer (Malvern Instruments, Ltd., UK). The abbreviations of various NCs were listed in Table S2.

To quantify the protein encapsulation efficiency, ^{Cy5}BSA-containing NCs (^{Cy5}BNCs or pHA@^{Cy5}BNCs) were prepared using the same method as described above. The NCs were subjected to ultrafiltration (MWCO = 100 kDa). The un-encapsulated ^{Cy5}BSA was collected and its concentration was determined by spectrofluorimetry (λ_{ex} = 633 nm, λ_{em} = 670 nm). Encapsulation efficiency was calculated using the following equation:

Encapsulation efficiency of BSA (%) = (total weight of ^{Cy5}BSA in feed - weight of un-encapsulated ^{Cy5}BSA) × 100/ total weight of ^{Cy5}BSA in feed.

To investigate the interaction between EGCG and BSA inside BNCs, Tween 20 (1 M in DI water, a hydrophobic interaction disruptor), urea (1 M in DI water, a hydrogen bonding disruptor), and phosphate buffer saline (PBS, an ionic interaction disruptor) were diluted with DI water to different concentrations (5, 10, 20, 50, and 100 mM) and mixed with BNCs (1 mL, containing 10 μg BSA and 3.5 μg EGCG) at the disruptor/BNCs volume ratio of 1/1. After incubation for 30 min, the particle size was measured by the Malvern Zetasizer.

2.5. Preparation and characterization of pHA-coated IL-22/BSA/EGCG nanocomplexes (pHA@IBNCs)

pHA@IBNCs were prepared using the similar method as described above. Briefly, IL-22 solution (1 mg/mL in DI water, 4 μL) was added into BSA solution (4 mg/mL in DI water, 1 mL) to obtain a mixed protein solution, followed by complexation with EGCG and surface-coating with pHA at the optimal BSA/IL-22/EGCG/pHA weight ratio of 1/0.001/0.35/1.25. The obtained pHA@IBNCs were subjected to ultrafiltration (MWCO = 100 kDa) to remove the un-encapsulated IL-22, BSA, or EGCG. The un-encapsulated IL-22 was collected and its concentration was determined by ELISA. Encapsulation efficiency of IL-22 was calculated using the same equation as described above.

The hydrodynamic size and zeta potential of pHA@IBNCs were determined by the Malvern Zetasizer, and the morphology was observed by transmission electron microscopy (TEM, TECNAI G2, FEI, USA).

To determine whether the nano-encapsulation process would damage the bioactivity of IL-22, pHA@IBNCs (1 μg IL-22/mL, 1 mL) were incubated with Tween 20 (100 mM, 1 mL) at 37 °C for 4 h to dissociate pHA@IBNCs and completely release IL-22. Free IL-22 (1 μg/mL, 1 mL) receiving the same treatment served as the control. The released IL-22 and free IL-22 at the same concentration were subjected to activity assessment using the ELISA kit, and results were presented as percentage activity of the control.

To evaluate the colloidal stability, pHA@IBNCs or IBNCs (1 μg IL-22/mL, 100 μL) were incubated in PBS (pH 7.4, 1 mL) containing 10 % FBS at 37 °C, and their particle sizes at different time points were determined.

To confirm the presence of the boronate bond between pHA and IBNCs, the fluorescence titration was further performed with IBNCs at incremental EGCG concentrations in the presence of a mixture of pHA (1×10^{-4} mol/L) and ARS (1×10^{-4} mol/L) in buffer (52.1 % methanol in DI water with 10 mmol/L KCl, 2.7 mmol/L KH_2PO_4, 2.7 mmol/L Na_2HPO_4, pH 8.21). The fluorescence emission spectra of the mixture were recorded within the range of 540–650 nm (λ_{ex} = 495 nm).

2.6. ROS-responsive NCs dissociation and IL-22 release

The H_2O_2-triggered removal of the surface-coated pHA from pHA@IBNCs was monitored by the fluorescence resonance energy transfer (FRET) assay. Briefly, ^{Cy5}pHA@I^{Cy3}BNCs comprised of ^{Cy5}pHA and ^{Cy3}BSA as the FRET pair were prepared as described above. After incubation with H_2O_2 (0.2 mM) for 30 min, the fluorescence emission spectra were collected within the range of 565–800 nm (λ_{ex} = 550 nm). To explore the RNS-triggered shedding of the pHA shells, the FRET assay was employed as describe above except that $ONOO^-$ (a typical reactive nitrogen species (RNS), 0.2 mM) was used instead of H_2O_2 [45].

To study the IL-22 release in response to ROS, freshly fabricated pHA@IBNCs (1 mL, containing 1 μg IL-22) were placed in a dialysis tube (MWCO = 300 kDa) and immersed in PBS (30 mL) supplemented with or without H_2O_2 (0.2 mM). After incubation at 37 °C for predetermined time intervals, an aliquot of the release medium (200 μL) was taken out and replenished with an equal volume of fresh medium. The concentration of IL-22 in the aliquot was determined by ELISA, and the cumulative release amount was calculated.

2.7. Anti-oxidant capabilities of pHA@IBNCs

The anti-oxidant capabilities of pHA@IBNCs were assessed in terms of the scavenging efficiencies for H_2O_2, ABTS radicals, and DPPH radicals.

For the assessment of the H_2O_2 scavenging capacity, EGCG, IBNCs, or pHA@IBNCs (0.14 μg IL-22/mL and 50 μg EGCG/mL) were added into H_2O_2 solution (0.2 mM) and incubated at room temperature for 2 h. The H_2O_2 concentrations before (C_0) and after (C_1) incubation with EGCG or NCs were determined using the H_2O_2 assay kit according to the manufacturer's instructions, and the H_2O_2-scavenging capacity was calculated using the following equation:

$$H_2O_2 - \text{scavenging capacity}\ (\%) = (C_0 - C_1) \times 100/C_0$$

The ABTS radical-scavenging assay was performed as described previously [46]. Firstly, ABTS stock solution (7 mM in ethanol) was incubated with potassium persulfate solution (2.45 mM in ethanol) at equal volume in the dark at 37 °C for 12 h to prepare the ABTS free radical solution. pHA@IBNCs at different concentrations were then added at the pHA@IBNCs/ABTS volume ratio of 1/30 and were incubated at 37 °C for 1 h. The absorbance of the ABTS radical solution at 734 nm before ($^{ABTS}OD_0$) and after ($^{ABTS}OD_1$) incubation with pHA@IBNCs was measured, and the ABTS radical-scavenging capacity was calculated using the following equation:

$$\text{ABTS radical} - \text{scavenging capacity}\ (\%) = \left(^{ABTS}OD_0 - {}^{ABTS}OD_1\right) \times 100/{}^{ABTS}OD_0$$

The DPPH radical-scavenging assay was also performed as described previously [47]. Briefly, pHA@IBNCs at different concentrations were added to the DPPH radical solution (0.1 mM in ethanol) at the pHA@IBNCs/DPPH volume ratio of 1/20 and were incubated at 37 °C for 1 h. The absorbance of the DPPH radical solution at 517 nm before ($^{DPPH}OD_0$) and after ($^{DPPH}OD_1$) incubation with pHA@IBNCs was measured, and the DPPH radical-scavenging capacity was calculated using the following equation:

$$\text{DPPH radical} - \text{scavenging capacity}\ (\%) = \left(^{DPPH}OD_0 - {}^{DPPH}OD_1\right) \times 100/{}^{DPPH}OD_0$$

2.8. pHA-mediated inflamed MIECs and macrophages targeting

To evaluate the pHA-mediated inflamed MIECs and RAW 264.7 cells targeting efficiency of pHA@IBNCs, MIECs or RAW 264.7 cells were seeded on 24-well plates at 1×10^5 cells/well and cultured for 12 h. After replacement with fresh medium, cells were challenged with LPS (2 μg/mL) for 24 h before addition of pHA@^{Cy5}IBNCs or ^{Cy5}IBNCs (0.14 μg ^{Cy5}IL-22/mL and 50 μg EGCG/mL) with or without free HA pretreatment (10 mg/mL, 4 h). After incubation at 37 °C for 4 h, cells were washed with cold PBS for three times and analyzed by flow cytometry (Beckton Dickinson, USA).

2.9. Anti-oxidant, anti-inflammatory, and cytoprotective efficiencies of pHA@IBNCs in MIECs and MPACs

To evaluate the anti-oxidant efficiency of pHA@IBNCs, MIECs or MPACs were seeded on glass-bottomed cell culture dish (Φ = 20 mm) at 1×10^5 cells/well and cultured for 12 h. After replacement with fresh medium, cells were incubated with PBS, pHA@IBNCs, IBNCs, or EGCG (0.14 μg IL-22/mL and 50 μg EGCG/mL) and challenged with H_2O_2 (0.2 mM) for 24 h before staining with DHE (5 μM, a ROS probe) at 37 °C for 30 min. After washing with cold PBS for three times, cells were observed by confocal laser scanning microscopy (CLSM, Zeiss LSM 800, λ_{ex} = 518 nm, λ_{em} = 616 nm), and the fluorescence intensities were determined using the ImageJ software. Results were denoted as percentage fluorescence intensity of PBS-treated cells. Cells treated with PBS yet without H_2O_2 challenge served as the control.

To evaluate the cytoprotective efficiency against ROS, MIECs or MPACs were seeded on 96-well plates at 1×10^4 cells/well and cultured for 12 h. After replacement with fresh medium, cells were incubated with PBS, pHA@IBNCs, IBNCs, or EGCG (0.14 μg IL-22/mL and 50 μg EGCG/mL) and challenged with H_2O_2 (0.2 mM) for 24 h before assessment of cell viability by the MTT assay. Results were represented as percentage viability of control cells that were treated with PBS yet without H_2O_2 challenge.

To evaluate the anti-inflammatory efficiency of pHA@IBNCs, MIECs

or MPACs were seeded on 24-well plates at 1×10^5 cells/well and cultured for 12 h. After replacement with fresh medium, cells were incubated with PBS, pHA@IBNCs, IBNCs, or EGCG (0.14 μg IL-22/mL and 50 μg EGCG/mL) and challenged with LPS (2 μg/mL) for 24 h before determination of pro-inflammatory cytokines (IL-6, IL-1β, and TNF-α) concentrations in the medium by using ELISA kits.

2.10. Establishment of STC-induced SAP mouse model

SAP mouse model was established as reported previously [48]. Briefly, anesthetized mice underwent a midline laparotomy and the papilla of Vater was identified. A puncture through the duodenal wall, opposite to the papilla of Vater, was performed under microscopic observation using a 30 G needle. A polyethylene catheter connected to a micro-infusion pump was inserted 1 mm into the common bile duct. STC (3.5 % in saline, 50 μL, containing methylene blue as a visual indicator) was infused into the pancreatic duct at the rate of 10 μL/min. The catheter and the bile duct clip were removed and the duodenal puncture was closed before suturing of the abdominal wall.

2.11. Pharmacokinetics and biodistribution of pHA@IBNCs

For the pharmacokinetics study, free ^{Cy5}IL-22, ^{Cy5}IBNCs, or pHA@-^{Cy5}IBNCs were *i.v* injected to healthy mice (10 μg ^{Cy5}IL-22/kg and 3.5 mg EGCG/kg). Blood (50 μL) was collected from the orbit at pre-determined time intervals and centrifuged at 3000 rpm for 5 min. The amount of ^{Cy5}IL-22 in the supernatant was quantified by spectrofluorimetry (λ_{ex} = 633 nm, λ_{em} = 670 nm).

For the biodistribution study, pHA@^{Cy5}IBNCs (10 μg ^{Cy5}IL-22/kg and 3.5 mg EGCG/kg) were *i.v* injected to SAP or healthy mice, while ^{Cy5}IBNCs (10 μg ^{Cy5}IL-22/kg and 3.5 mg EGCG/kg) were *i.v* injected to SAP mice. Mice were sacrificed at 4 h post administration. The major organs (heart, liver, spleen, lung, kidney, pancreas, and colon) were harvested and imaged using the *In-Vivo* Imaging System (Cambridge Research and Instrumentation, Inc., λ_{ex} = 633 nm, λ_{em} = 670 nm).

2.12. Therapeutic efficacy of pHA@IBNCs in STC-induced SAP mice

Many prognostication models have been developed to predict SAP at the early stage, and thus early management (*e.g.* fluid resuscitation, nutritional support, and analgesia) in predicted SAP patients has been demonstrated beneficial for the disease treatment [49,50]. To simulate these clinical scenarios, in the current study, mice were *i.v.* injected with PBS, EGCG, IL-22, pHA@BNCs, or pHA@IBNCs (10 μg IL-22/kg and 3.5 mg EGCG/kg) at −48, −24, 0, 2, and 4 h post STC challenge. The survival rate of mice was monitored from 0 to 24 h. At 24 h post STC challenge, blood was collected from the orbit, and the pro-inflammatory cytokine (IL-6, IL-1β, and TNF-α) levels as well as amylase activity in the serum were determined using commercial kits. Mice were then sacrificed, and the pancreas tissue was harvested to determine the mRNA levels of pro-inflammatory cytokines (IL-6, IL-1β, and TNF-α) by real-time PCR. Briefly, the pancreas tissue (10 mg) was homogenized with the Trizol reagent (1 mL) to isolate total RNA, and cDNA was synthesized from total RNA using the high-capacity cDNA reverse transcription kit according to the manufacturer's instruction. Synthesized cDNA, primers (forward and reverse), and SYBR Premix Ex Taq were mixed and run on the real-time PCR system (CFX connect, S9 Bio-Rad). All samples were analyzed for β-actin in the same run. In parallel, the pancreas tissue (10 mg) was homogenized with the passive lysis buffer. The homogenate was centrifuged at 13000 rpm and 4 °C for 10 min before quantification of MPO and H_2O_2 levels in the supernatant using commercial assay kits.

2.13. Efficacy of pHA@IBNCs in restoring intestinal barrier in SAP mice

SAP mice received the same drug administration as described above. Mice were sacrificed at 24 h post STC challenge. The colon tissue (10 mg) was harvested and rinsed with PBS. The mRNA levels of pro-inflammatory cytokine (IL-6, IL-1β, and TNF-α) and epithelial tight junction markers (ZO-1 and Occludin) were determined by real-time PCR. The MPO activity and H_2O_2 level in mouse colon were determined as described above. ZO-1, Occludin, STAT3, phospho-STAT3 (p-STAT3), Lgr5, and PCNA protein levels in colon were further evaluated by Western blot analysis with α-tubulin as the internal control. Briefly, the harvested colon tissue (10 mg) was lysed with the RIPA lysis buffer, mixed with the SDS-PAGE protein loading buffer, incubated at 95 °C for 5 min, and subjected to Western blot analysis. The concentrations of primary antibodies were as follow, anti-ZO-1 (Abcam, 1:2000), anti-Occludin (Abcam, 1:1000), anti-STAT3 (Cell Signaling Technology, 1:1000), anti-p-STAT3 (Cell Signaling Technology, 1:1000), anti-Lgr5 (Abcam, 1:1000), and anti-PCNA (Cell Signaling Technology, 1:1000). The concentrations of secondary antibodies were as follow, goat-anti-rabbit IgG (Abcam, 1:1000) and goat-anti-mouse IgG (Abcam, 1:1000). The intestinal permeability was further evaluated using FITC-dextran (4 kDa) as described previously [51]. Briefly, at 24 h post STC challenge, mice were orally gavaged with FITC-dextran at 600 mg/kg. Blood was collected 4 h later, and the FITC-dextran content in the serum was determined by spectrofluorimetry (λ_{ex} = 488 nm, λ_{em} = 520 nm).

2.14. Hematoxylin and eosin (H&E) staining

SAP mice received the same drug administration as described above. Mice were sacrificed at 24 h post STC challenge, and the pancreas and colon tissues were harvested, fixed in 10 % neutral buffered formalin, embedded in paraffin, sectioned at 8 μm in thickness, and stained with H&E followed by histological observation using optical microscopy. Pancreatic interstitial edema, acinar cell necrosis, leukocyte infiltration, and hemorrhage were scored according to the Schmidt scoring criteria [52].

2.15. Immunofluorescence staining

SAP mice received the same drug administration as described above. Mice were sacrificed at 24 h post STC challenge, and the colon tissues were harvested, dehydrated in 30 % (*w/v*) sucrose solution overnight, embedded in OCT at −80 °C, and cryosectioned at 15 μm in thickness. The sections were fixed in iced acetone for 5 min, rinsed with PBS for three times, and then immunofluorescence staining was carried out through the following steps, including blocking with 5 % BSA for 2 h, incubation with primary antibody at 4 °C overnight, incubation with secondary antibody for 1 h at room temperature, and staining with DAPI (10 μg/mL) for 10 min. The concentrations of primary antibodies were as follow, anti-cytokeratin 18 (CK18, Immunoway, 1:200) and anti-Ki67 (Abcam, 1:200). The concentrations of secondary antibodies were as follow, FITC-goat-anti-rabbit IgG (Abcam, 1:50) and Cy5-goat-anti-mouse IgG (Abcam, 1:50). The tissue sections were then observed by CLSM.

2.16. Biocompatibility evaluation

Healthy mice were *i.v.* injected with pHA@IBNCs (10 μg IL-22/kg and 3.5 mg EGCG/kg) for five times with 12 h spaced between each injection. At 24 h post the last injection, blood was collected and subjected to hematological and biochemical analyses using the Cobas501 automatic hematology analyzer (Roche, USA) and BC-5380 automatic chemistry analyzer (Mindray, China), respectively. Mice injected with PBS served as the control. In addition, the heart, liver, spleen, lung, kidney, pancreas, and colon were collected and subjected to H&E staining and histological observation.

2.17. Statistical analysis

Statistical analysis was conducted using the two-tailed Student's *t*-

test, and differences between two groups with unpaired biological replicates were judged to be significant at $^{*}P < 0.05$ and very significant at $^{**}P < 0.01$ and $^{***}P < 0.001$.

3. Results and discussion

3.1. Synthesis of pHA

ABA was conjugated to HA in a mixed solvent of water and ethanol *via* the EDC/NHS coupling reaction, and the chemical structure of pHA was confirmed by ^{1}H NMR (Fig. S1). An average of 6.7 ABA molecules was conjugated onto each HA molecule, as calculated by comparing the integration areas of the phenyl protons in ABA (δ, 7.7–7.3 ppm) and the protons of the *N*-acetyl group in HA (δ, 1.8 ppm).

3.2. Preparation and characterization of pHA@IBNCs

EGCG and BSA were mixed to form the BNCs. Particle size of the BNCs gradually increased from 43 to 288 nm at increased EGCG/BSA weight ratio from 0.05 to 0.7 (Fig. 1A). To investigate the interactions between EGCG and BSA, the size change of BNCs after incubation with different disruptors was monitored. As shown in Fig. S2, BNCs were dissociated by Tween 20 (a hydrophobic interaction disruptor) and urea (a hydrogen bonding disruptor), while maintained integral after incubation in PBS (an ionic interaction disruptor), indicating that both hydrogen bonding and hydrophobic interaction drove the formation of BNCs. The pHA@BNCs were then constructed *via* covalent coating of BNCs with pHA, wherein boronate ester bonds were formed between the catechol moieties in EGCG and the pendant phenylboronic acids in pHA. The addition of pHA did not notably increase the particle size of the pHA@BNCs when the pHA/BSA weight ratio was below 1.25, while an obvious increase indicative of aggregation was observed when the pHA/BSA weight ratio reached 2.5 (Fig. 1A). All pHA@BNCs possessed negative zeta potentials around −18 mV (Fig. 1B). The encapsulation efficiency of BSA in pHA@BNCs reached >90 % at the BSA/EGCG ratio ≥ 0.35, mainly owing to the hydrogen bonding between protein and polyphenol (Fig. 1C). Therefore, the optimal BSA/EGCG/pHA weight ratio of 1/0.35/1.25 was adopted to fabricate pHA@BNCs for further studies, which adopted the particle size of ~150 nm and BSA encapsulation efficiency of ~95 %.

Then, pHA@IBNCs were similarly synthesized from IL-22, BSA, EGCG, and pHA at the BSA/IL-22/EGCG/pHA weight ratio of 1/0.001/0.35/1.25. As shown in Fig. S3 and S4, the freshly prepared pHA@IBNCs possessed the hydrodynamic diameter of ~180 nm, negative zeta potential of ~ − 18 mV, and high IL-22 encapsulation efficiency of ~95 %. TEM image revealed the spherical morphology of pHA@IBNCs with the diameter of ~150 nm (Fig. 1D). After incubation in PBS (pH 7.4) containing 10 % FBS for up to 24 h, the size of pHA@IBNCs remained almost unaltered while that of IBNCs gradually increased to 300 nm (Fig. S5). Such discrepancy was mainly because pHA coating formed a hydrophilic corona to prevent adsorption of serum proteins onto the surface of polyphenols-constituted NCs. IL-22 encapsulated in pHA@IBNCs showed comparable activity to free IL-22 (Fig. S6), indicating that the nano-assembly process would not impair the activity of IL-22.

To verify the successful coating of pHA on the surface of IBNCs through the boronate ester bond, the ARS binding assay was performed (Fig. S7a). The mixture of ARS and pHA displayed pronounced fluorescence at 580 nm due to the binding of catechol in ARS and boronic acid in pHA, indicating the formation of boronate ester. With the addition of IBNCs, the fluorescence intensity decreased dramatically and gradually approached the ARS baseline when the IBNCs concentration reached 150 μg EGCG/mL (Fig. S7b). This phenomenon was attributed to the competitive binding of the catechol in IBNCs to the phenylboronic acid in pHA, resulting in the release of more free ARS into solution and hence a decrease in fluorescence.

3.3. ROS-responsive pHA shedding from pHA@IBNCs and IL-22 release

The boronate ester bonds formed between pHA and EGCG can be readily broken by the over-produced H_2O_2 in the inflammatory microenvironment, thereby driving the removal of pHA and exposure of the IBNCs. To explore the shedding of the pHA shell, the FRET assay was first performed on ^{Cy5}pHA@I^{Cy3}BNCs comprised of ^{Cy3}BSA (donor) and ^{Cy5}pHA (acceptor). Pronounced FRET effect was noted for ^{Cy5}pHA@I-^{Cy3}BNCs, as evidenced by the fluorescence intensity increase at 670 nm (Cy5) yet decrease at 560 nm (Cy3). Whereas, the FRET effect was obviously weakened after addition of H_2O_2, indicating ROS-triggered detachment of pHA from pHA@IBNCs (Fig. 1E). The weakened FRET

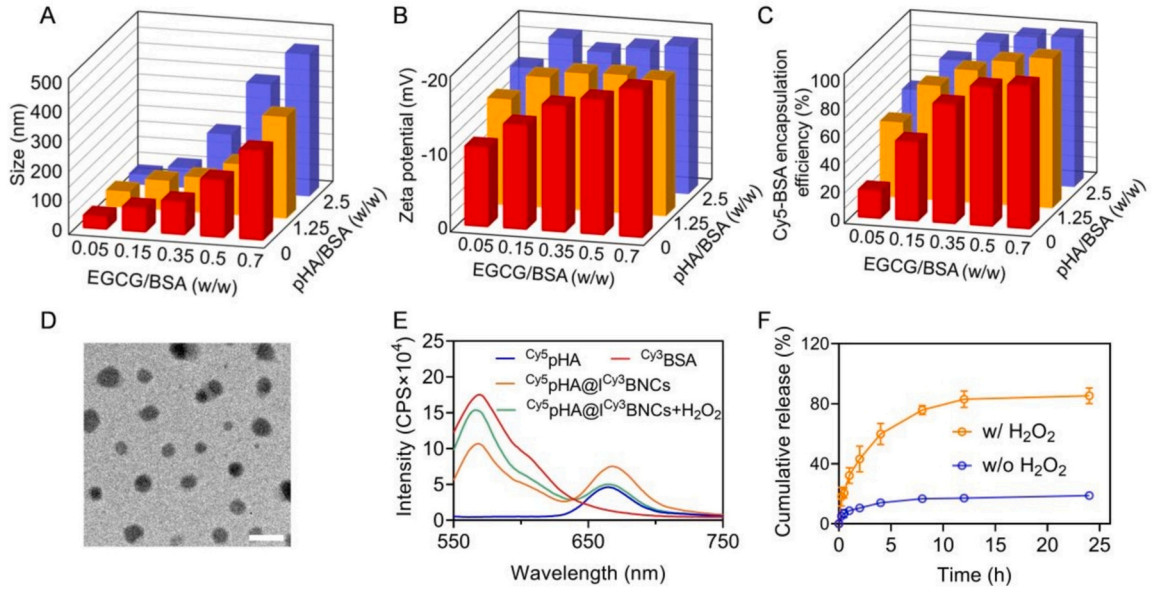

Fig. 1. Characterization of pHA@IBNCs. Size (A), zeta potential (B), and BSA encapsulation efficiency (C) of pHA@BNCs prepared at various EGCG/BSA and pHA/BSA weight ratios ($n = 3$). (D) TEM image of pHA@IBNCs (scale bar = 500 nm). (E) Fluorescence emission spectra of ^{Cy5}pHA, ^{Cy3}BSA, ^{Cy5}pHA@I^{Cy3}BNCs, and H_2O_2-treated (0.2 mM, 30 min) ^{Cy5}pHA@I^{Cy3}BNCs (excitation for Cy3 at 550 nm). (F) Cumulative release of IL-22 from pHA@IBNCs in PBS with (w/) or without (w/o) H_2O_2 (0.2 mM, $n = 3$). Data were presented as mean ± standard deviation (s.d.).

effect was also noted after $ONOO^-$ (other important participants of oxidative stress) treatment, further demonstrating the RNS-responsive of pHA@IBNCs (Fig. S8). TEM image revealed the dissociation of pHA@IBNCs, as evidenced by the disappeared spherical morphology of NCs after H_2O_2 treatment (Fig. S9). In accordance, IL-22 release from pHA@IBNCs was greatly enhanced by H_2O_2 (Fig. 1F). In the absence of H_2O_2, IL-22 release was slow, reaching the accumulative release amount of only ~10 % within 24 h. In comparison, in the presence of H_2O_2 (0.2 mM), a quicker IL-22 release of ~50 % within the first 4 h was noted, which then slowly reached equilibrium (~80 %) in the following 8 h.

3.4. The CD44 targeting capacity of pHA@IBNCs

The CD44 targeting capability of pHA@IBNCs were evaluated in LPS-challenged MIECs and RAW 264.7 cells. As shown in Fig. S10, pHA@IBNCs showed notably higher cell uptake level than IBNCs in MIECs or RAW 264.7 cells. When cells were pre-treated with free HA to block the CD44 on cell surfaces, the uptake level of pHA@IBNCs but not IBNCs in MIECs or RAW 264.7 cells was dramatically reduced, demonstrating that the pHA coating could facilitate the accumulation of NCs to the inflamed MIECs and activated macrophages through the interaction between pHA and CD44.

3.5. Anti-oxidant, anti-inflammatory, and cytoprotective capabilities of pHA@IBNCs in vitro

The H_2O_2 scavenging assay was then performed to evaluate the anti-oxidant capacity of pHA@IBNCs. As illustrated in Fig. 2A, ~70 % of H_2O_2 was decomposed after incubation with pHA@IBNCs for 2 h, significantly outperforming EGCG (~20 %) and IBNCs (~20 %). The free radical scavenging capacity of pHA@IBNCs was further evaluated using the ABTS and DPPH radical assays. pHA@IBNCs exhibited a concentration-dependent manner in quenching both ABTS and DPPH radicals, correspondingly showing the color change from green or blue to colorless in the solution (Fig. S11). Moreover, pHA@IBNCs (1.5 mg/mL) achieved the ABTS and DPPH scavenging rates of ~80 % and ~ 95

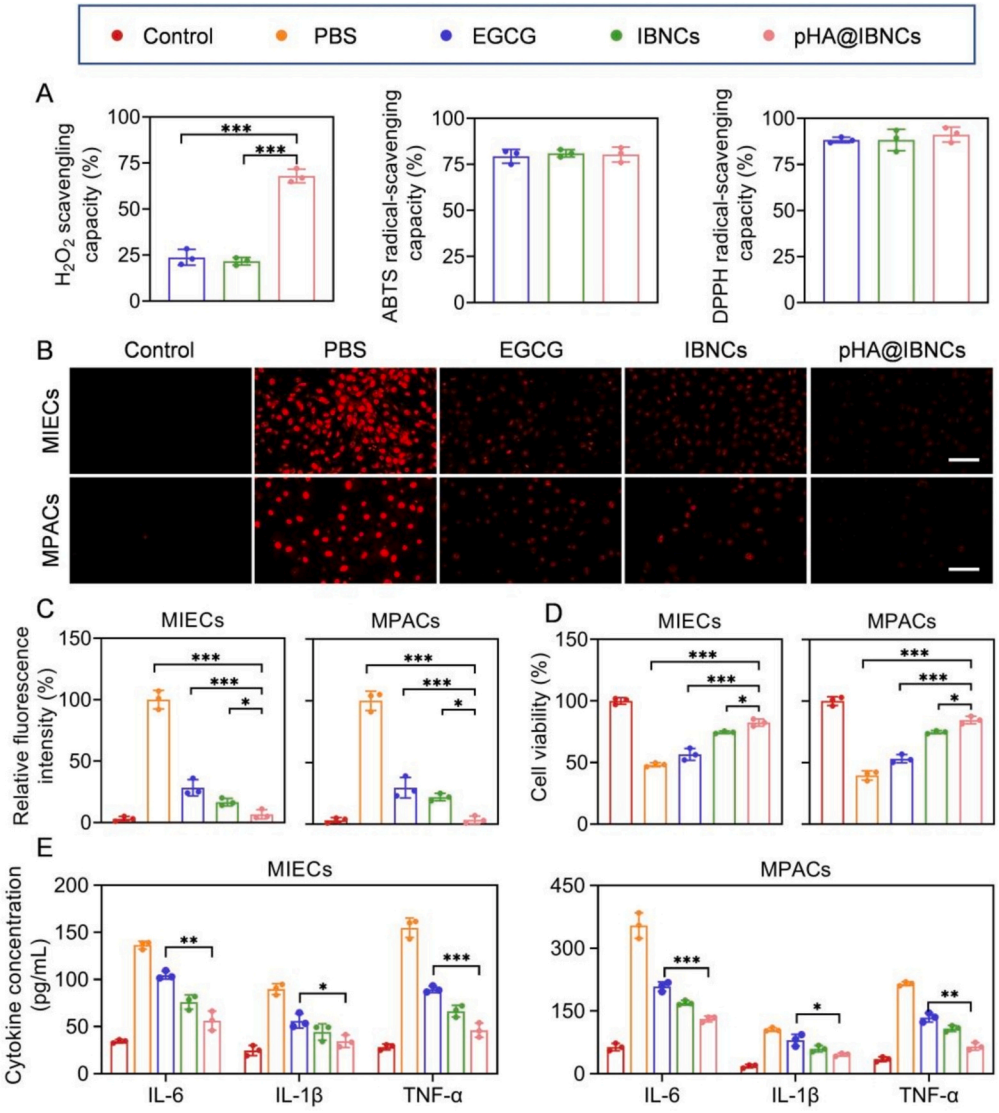

Fig. 2. Anti-oxidant, anti-inflammatory, and cytoprotective capabilities of pHA@IBNCs *in vitro*. (A) H_2O_2, ABTS, and DPPH scavenging capacities of EGCG or NCs ($n = 3$). (B) CLSM images of MIECs and MPACs after incubation with EGCG or NCs in the presence of H_2O_2 (0.2 mM). Cells were stained with DHE (a ROS probe) before observation (scale bar = 50 μm). (C) Relative fluorescence intensities of MIECs and MPACs calculated from (B) ($n = 3$). Fluorescence intensities of cells treated with PBS in the presence of H_2O_2 (0.2 mM) served as 100 %. (D) Viabilities of MIECs and MPACs treated with EGCG or NCs in the presence of H_2O_2 (0.2 mM, $n = 3$). Viability of control cells served as 100 %. (E) Extracellular pro-inflammatory cytokine concentrations of MIECs and MPACs after incubation with EGCG or NCs in the presence of LPS (2 μg/mL, $n = 3$). In (B-E), cells treated with PBS yet without H_2O_2 or LPS challenge served as the control. Data were presented as mean ± s.d..

%, respectively (Fig. 2A), in similar capacity to free EGCG and IBNCs.

The intestinal epithelium and pancreatic acinar cells are susceptible to damage by oxidative stress. Then, the anti-oxidant efficiencies of NCs were further monitored in H_2O_2-challenged MIECs and MPACs by employing the ROS probe (DHE). pHA@IBNCs provoked the highest ROS scavenging efficiencies of ~93 % and ~ 96 % in MIECs and MPACs, respectively, significantly outperforming EGCG and IBNCs (Fig. 2B and C). These results therefore demonstrated that the degradation of boronate ester bonds could consume H_2O_2 and cooperate with EGCG-mediated superoxide radical reduction to scavenge ROS. As a consequence, pHA@IBNCs revealed pronounced cytoprotective effect, outperforming free EGCG and IBNCs to dramatically increase the viability of H_2O_2-challenged MIECs and MPACs (Fig. 2D). Moreover, pHA@IBNCs and IBNCs outperformed EGCG to remarkably downregulate the IL-6, IL-1β, and TNF-α secretion levels in LPS-challenged MIECs and MPACs, which evidenced the important contribution of IL-22 in attenuating inflammation (Fig. 2E).

3.6. Pharmacokinetics and biodistribution

The pharmacokinetics of ^{Cy5}IL-22, ^{Cy5}IBNCs, and pHA@^{Cy5}IBNCs were evaluated in healthy mice following *i.v.* injection. As shown in Fig. 3A, ^{Cy5}IBNCs and pHA@^{Cy5}IBNCs showed markedly prolonged circulation time than free ^{Cy5}IL-22, and the blood circulation half-life ($t_{1/2}$) of pHA@^{Cy5}IBNCs ($t_{1/2}$ = 4.78 h) was ~2.1-fold longer than that of ^{Cy5}IBNCs ($t_{1/2}$ = 2.33 h). Such enhancement was mainly attributed to the surface decoration of pHA that hindered the absorption of serum proteins onto ^{Cy5}IBNCs and accordingly reduced the clearance by reticuloendothelial tissues.

To assess the ability of pHA@IBNCs in targeting the inflamed lesions, SAP mouse model was established by retrograde infusion of STC into the pancreatic duct. As indicated in Fig. 3B and C, pHA@IBNCs showed significantly higher accumulation levels than IBNCs in the pancreas and colon of SAP mice. Moreover, pHA@IBNCs showed 2.8- and 1.5-fold higher distribution levels in the pancreas and colon of SAP mice than that of healthy mice. Such observation thus demonstrated that pHA@IBNCs were preferentially enriched in the inflamed tissues, possibly due to the binding of pHA onto overexpressed CD44 on the surfaces of IECs in the inflamed colon and activated macrophages in the inflamed pancreas and colon.

3.7. pHA@IBNCs-mediated inhibition of inflammation and acinar cell injury in vivo

The therapeutic efficacy of the pHA@IBNCs against SAP was evaluated after five injections at −48, −24, 0, 2, and 4 h post STC challenge (Fig. 4A). SAP mice receiving PBS injection showed mortality of 30 % within 24 h upon STC challenge, while mice treated with pHA@IBNCs revealed 100 % survival (Fig. 4B). The anti-oxidant and anti-inflammatory efficacies of pHA@IBNCs were further investigated. Consistent with the *in vitro* results, pHA@IBNCs outperformed pHA@BNCs and free drugs to notably decrease the H_2O_2 level (Fig. 4C),

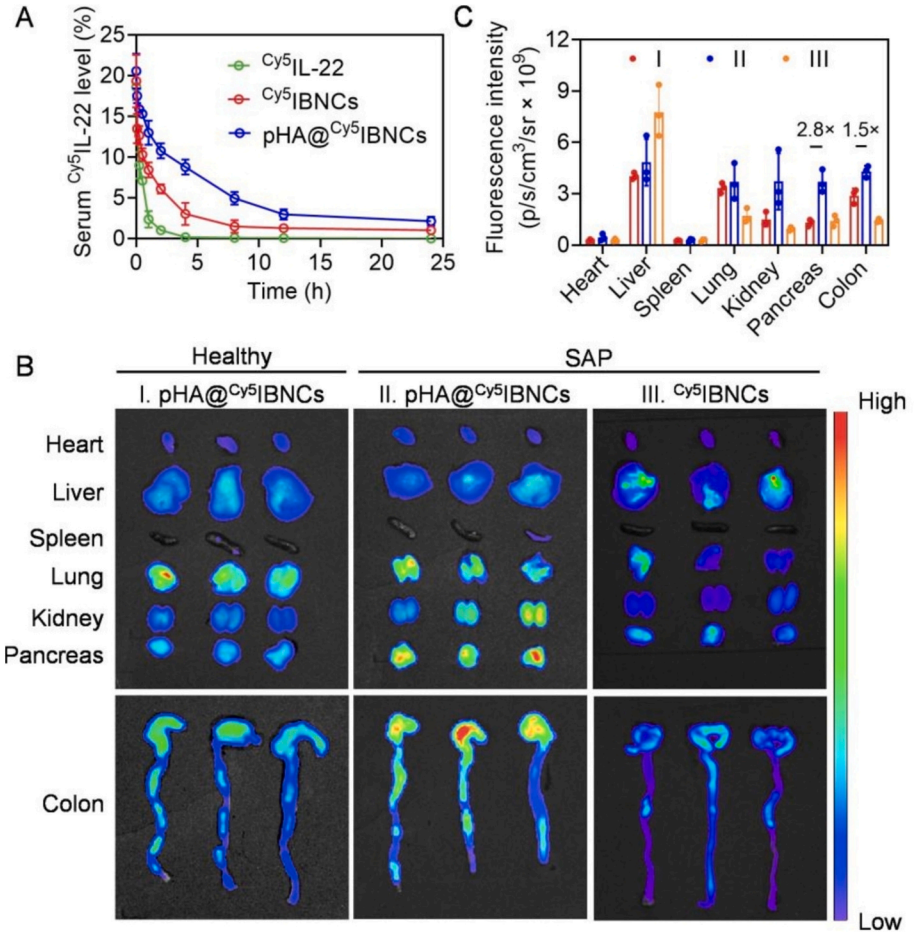

Fig. 3. Pharmacokinetics and biodistribution of pHA@IBNCs. (A) Serum ^{Cy5}IL-22 levels in healthy mice at different time points post *i.v.* injection of ^{Cy5}IL-22, ^{Cy5}IBNCs, or pHA@^{Cy5}IBNCs at 10 μg ^{Cy5}IL-22/kg and 3.5 mg EGCG/kg (n = 3). *Ex vivo* fluorescence images (B) and quantified fluorescence intensities (C) of major organs of healthy or SAP mice at 4 h post *i.v.* injection of pHA@^{Cy5}IBNCs or ^{Cy5}IBNCs at 10 μg ^{Cy5}IL-22/kg and 3.5 mg EGCG/kg (n = 3). Data were presented as mean ± s.d..

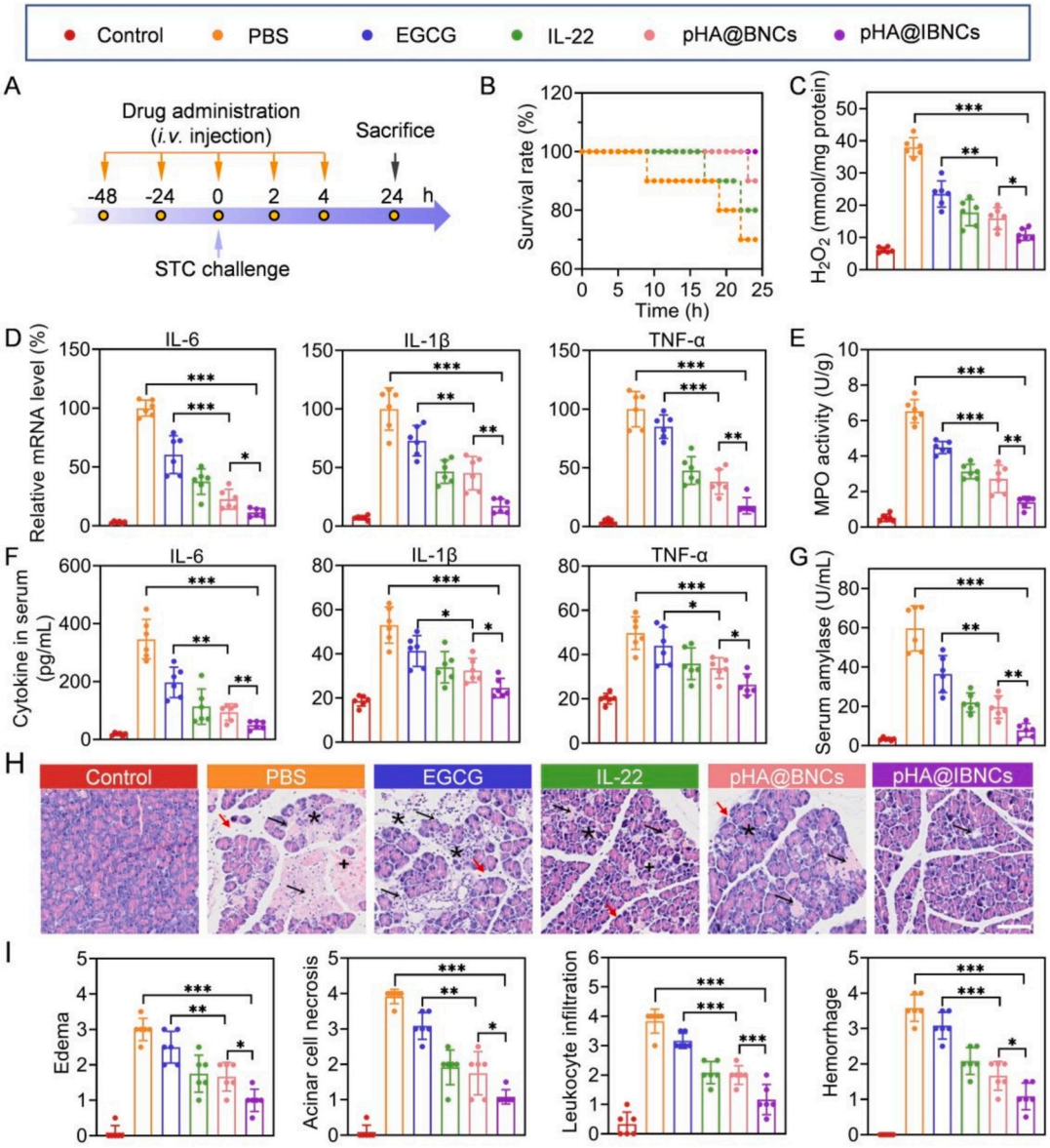

Fig. 4. Anti-oxidant and anti-inflammatory efficacies of pHA@IBNCs in SAP mice. (A) Workflow of the animal study. Mice were challenged with STC (3.5 % in saline, 50 μL) *via* pancreatic duct infusion at 0 h to induce SAP, and were *i.v.* injected with PBS, free drugs (EGCG or IL-22), pHA@BNCs, or pHA@IBNCs at −48, −24, 0, 2, and 4 h at 10 μg IL-22/kg and 3.5 mg EGCG/kg. Healthy mice without STC challenge served as the control. Analyses in (C—I) were performed at 24 h post STC challenge. (B) Survival rate of mice within the observation period from 0 to 24 h. H_2O_2 level (C), relative mRNA levels of pro-inflammatory cytokines (D), and MPO activity (E) in mouse pancreas ($n = 6$). Serum levels of pro-inflammatory cytokines (F) and amylase (G) ($n = 6$). (H) Representative images of H&*E*-stained pancreatic sections (scale bar = 100 μm). The black arrow, red arrow, asterisk, and plus point to acinar necrosis, edema, cell infiltration, and hemorrhage, respectively. (I) Quantitative histological scores of edema, acinar cell necrosis, leukocyte infiltration, and hemorrhage from H&E-stained pancreatic sections ($n = 6$). Data were presented as mean ± s.d.. (For interpretation of the references to color in this figure legend, the reader is referred to the web version of this article.)

mRNA levels of several pro-inflammatory cytokines (IL-6, IL-1β, and TNF-α, Fig. 4D), and activity of MPO (an enzyme positively correlated with neutrophil activity, Fig. 4E) in the pancreatic tissue, indicating alleviation of oxidative stress and local inflammation in the pancreas. Serum levels of pro-inflammatory cytokines (IL-6, IL-1β, and TNF-α) were also remarkably reduced, indicating inhibition of systemic inflammation (Fig. 4F). Moreover, after administration of pHA@IBNCs, the serum concentration of amylase, a clinical index of pancreatic function, almost recovered to the normal value, indicating pronounced diminishment of pancreatic damage (Fig. 4G). Such observation was further supported by the histological analysis of pancreas sections, which revealed that pHA@IBNCs notably relieved the edema, acinar cell necrosis, leukocyte infiltration, and hemorrhage (Fig. 4H and I). Taken together, these results demonstrated the desired efficacy of pHA@IBNCs in mitigating pancreatic inflammation and damage.

3.8. pHA@IBNCs attenuate SAP-associated intestinal injury and restore intestinal barrier

We further examined the performance of pHA@IBNCs in restoring the intestinal barrier in SAP mice. In consistence with the above findings, pHA@IBNCs remarkably downregulated the H_2O_2 level, pro-inflammatory cytokine mRNA levels, and MPO activity in colonic tissues (Fig. 5 A-C), indicating the mitigation of oxidative stress, inflammation, and neutrophil infiltration in colon. To further explore the protective effect of pHA@IBNCs on the intestinal barrier, the expression levels of tight junction-associated proteins (ZO-1 and Occludin) in colon were first determined by Western blot. As shown in Fig. 5D, the

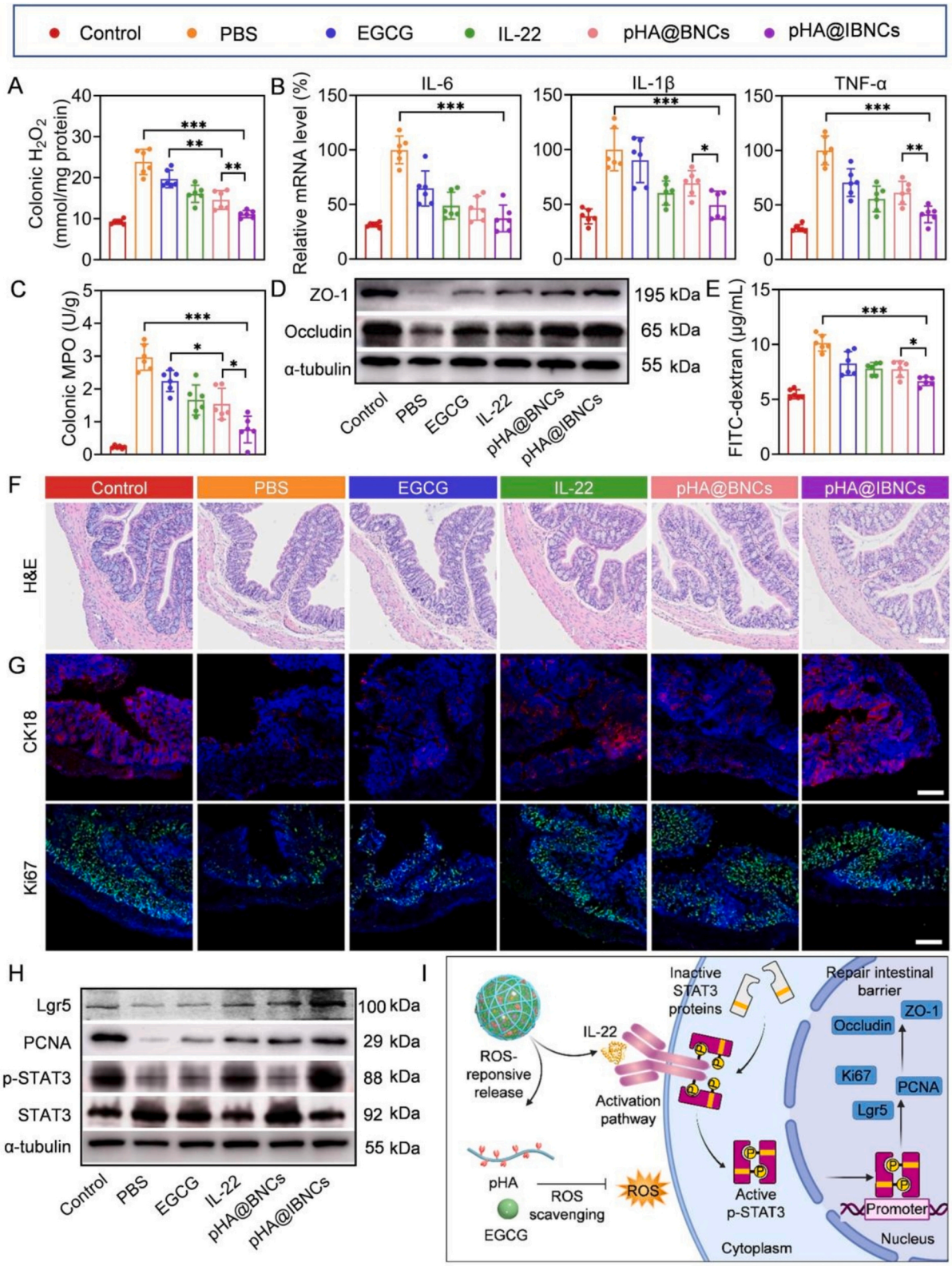

Fig. 5. pHA@IBNCs restore the intestinal barrier in SAP mice. H_2O_2 level (A), relative mRNA levels of pro-inflammatory cytokines (B), and MPO activity (C) in mouse colon ($n = 6$). (D) Western blot analysis of ZO-1 and Occludin expression in mouse colon. (E) Serum FITC-dextran concentration at 4 h post oral gavage of FITC-dextran ($n = 6$). (F) Representative images of H&E-stained colon sections (scale bar = 100 μm). (G) Representative images of colon sections immuno-stained for CK18 and Ki67 (scale bar = 100 μm). (H) Western blot analysis of Lgr5, PCNA, STAT3, and p-STAT3 expression in mouse colon. (I) Mechanisms of pHA@IBNCs-mediated intestinal barrier protection. Healthy mice without STC challenge served as the control. Analyses in (A-D and F-H) and FITC-dextran administration in (E) were performed at 24 h post STC challenge. Data were presented as mean ± s.d..

downregulation of ZO-1 and Occludin observed in the colon of SAP mice was significantly rectified after pHA@IBNCs treatment. In consistence, ZO-1 and Occludin mRNA levels nearly recovered to the normal levels of healthy mice (Fig. S12). Then, integrity of the intestinal barrier was assessed by using FITC-dextran, a macromolecule that is impermeable to the integral intestine with intact tight junctions [53]. Compared to that in PBS-treated SAP mice, serum FITC-dextran concentration in mice treated with pHA@IBNCs was obviously reduced, demonstrating restoration of the intestinal barrier (Fig. 5E). Histological analysis of H&E-stained colon sections further revealed notable alleviation of necrosis, mucosal membrane damage, destruction of crypt structure, and inflammatory cell infiltration after pHA@IBNCs treatment (Fig. 5F). Moreover, as revealed by immunofluorescence staining, the expression levels of CK18 (an epithelial cell protein that can be enzymatically digested in the apoptotic cells) and Ki67 (proliferation-associated protein) in pHA@IBNCs-treated colon tissues were greatly higher than those in PBS-treated colon tissues, indicating that pHA@IBNCs could effectively suppress apoptosis and promote regeneration of the colonic epithelia (Fig. 5G). IL-22 has been reported to promote the proliferation and expansion of ISCs by activating STAT3 phosphorylation [54]. In consistence with these reports, pHA@IBNCs herein notably upregulated the phosphorylation of STAT3, as resolved by Western blot analysis (Fig. 5H). As a consequence, the expression levels of Lgr5 (marker for ISCs) and PCNA (marker for the proliferative capacity of intestinal cells) were also upregulated by pHA@IBNCs (Fig. 5H). These results collectively indicated that pHA@IBNCs could prevent the SAP-induced intestinal damage by reducing the oxidative stress, inhibiting inflammatory responses, and promoting the intestinal cell proliferation (Fig. 5I).

3.9. Biocompatibility of pHA@IBNCs

The biocompatibility of pHA@IBNCs was evaluated in healthy mice following five *i.v.* injections with 12 h spaced between each injection. Compared to PBS-treated mice, pHA@IBNCs-treated mice showed negligible abnormalities in the context of representative hematological and blood biochemical parameters (Fig. S13 and S14). In addition, H&E-stained major organ sections revealed minimal abnormalities (Fig. S15). It therefore demonstrated the low systemic toxicity of pHA@IBNCs.

4. Conclusion

To date, effective therapeutic agents for the direct treatment or prevention of SAP are still lacking. Many studies on the pathogenesis of pancreatitis reveal that ROS play an important role in the pathological process of pancreatitis. Some preclinical treatment studies have also shown that ROS-scavenging nanotherapeutics have modest therapeutic effects in animal models [55–57]. However, a recent double-blind, placebo-controlled, randomised pilot study showed that single supplementation with the antioxidant agent, *N*-acetylcysteine, did not confer additional therapeutic benefit on endocrine and exocrine function, fibrosis progression, or inflammation severity in pancreatitis [58]. These evidences imply that single drug might not be sufficient to manage SAP owing to a variety of complex pathologies. Thus, inflammation-targeted and ROS-responsive pHA@IBNCs were developed for IL-22/EGCG co-delivery and SAP management. Based on pHA-mediated CD44 targeting, pHA@IBNCs could efficiently accumulate at the inflamed pancreas and colon, wherein the over-produced H_2O_2 disrupted the boronate ester bonds to shed off the pHA shell and promote the drug release. Thereafter, EGCG efficiently scavenged ROS and protected cells from apoptosis, while IL-22 blocked pro-inflammatory cytokines secretion and promoted proliferation of intestinal epithelial cells. These properties cooperated to attenuate inflammation and promote intestinal barrier repair in SAP mice. This study offers a facile and effective approach for the targeted delivery of anti-inflammatory and anti-oxidant pharmaceuticals. It also provides promising additions to the current therapeutic concepts against SAP, highlighting the importance to manage multi-organ crosstalk and target multiple events during disease progression. Compared to conventional drug delivery platforms for SAP treatment, firstly, pHA@IBNCs were prepared by simple self-assembly of natural, low-immunogenic components, thus offering the advantages of large-scale preparation and good biocompatibility [59,60]. Secondly, compared to the passive accumulation of drugs to the lesion site, pHA@IBNCs enabled active and selective accumulation to the inflammatory microenvironment, which may be conducive to the precise treatment of SAP. Finally, in contrast to single drug delivery systems, pHA@IBNCs as carriers also have a therapeutic effect on ROS-scavenging and can synergize the anti-SAP effect of protein drugs (*e.g.* interleukins, antibodies, or peptides). Obviously, as an emerging field, nanomedicine requires more clinical tests, longer observations, and persistent efforts. Future works require deeper insights into the SAP-related pathological events (*e.g.* premature trypsinogen activation, pathological calcium overload, pancreatic microcirculation disorders, infiltration of leucocyte cells, and impaired autophagy) [1,7]. Moreover, it will also be important to establish and validate animal models that can closely mimic key features of human pancreatitis. With these in mind, we expect pHA@IBNCs to be a useful tool for developing therapies for SAP and other related medical conditions.

CRediT authorship contribution statement

Juanhui Lin: Writing – original draft, Software, Methodology, Investigation. **Yuansong Wei:** Writing – review & editing, Investigation, Data curation, Conceptualization. **Xiaxian Gu:** Investigation, Data curation. **Miaoru Liu:** Data curation. **Mengru Wang:** Investigation. **Renxiang Zhou:** Software, Investigation. **Duowu Zou:** Software. **Lichen Yin:** Writing – review & editing, Supervision, Funding acquisition, Conceptualization. **Chunhua Zhou:** Writing – review & editing, Supervision, Funding acquisition, Conceptualization. **Duanmin Hu:** Writing – review & editing, Supervision, Funding acquisition, Conceptualization.

Declaration of competing interest

The authors declare no competing financial interest.

Acknowledgements

The authors acknowledge the financial support from the National Natural Science Foundation of China (81800570, 52273144, 52325305, and 52033006), Collaborative Innovation Center of Suzhou Nano Science & Technology, Gusu Health Talent Development Project (GSWS2020026), Suzhou Science and Technology Development Project (SKY2021044), the 111 Project, Suzhou Key Laboratory of Nanotechnology and Biomedicine, and Joint International Research Laboratory of Carbon-Based Functional Materials and Devices.

Appendix A. Supplementary data

Supplementary data to this article can be found online at https://doi.org/10.1016/j.jconrel.2024.11.022.

Data availability

Data will be made available on request.

References

[1] L. Boxhoorn, R.P. Voermans, S.A. Bouwense, M.J. Bruno, R.C. Verdonk, M. A. Boermeester, H.C. van Santvoort, M.G. Besselink, Acute pancreatitis, Lancet 396 (10252) (2020) 726–734.
[2] Y. Wang, X. Wang, X. Zhang, B. Zhang, X. Meng, D. Qian, Y. Xu, L. Yu, X. Yan, Z. He, Inflammation and acinar cell dual-targeting nanomedicines for synergistic

treatment of acute pancreatitis *via* Ca^{2+} homeostasis regulation and pancreas autodigestion inhibition, ACS Nano 18 (8) (2024) 11778–11803.
[3] S. Li, H. Li, H. Zhangdi, R. Xu, X. Zhang, J. Liu, Y. Hu, D. Ning, S. Jin, Hair follicle-MSC-derived small extracellular vesicles as a novel remedy for acute pancreatitis, J. Control. Release 352 (2022) 1104–1115.
[4] M.S. Petrov, S. Shanbhag, M. Chakraborty, A.R.J. Phillips, J.A. Windsor, Organ failure and infection of pancreatic necrosis as determinants of mortality in patients with acute pancreatitis, Gastroenterology 139 (3) (2010) 813–820.
[5] Y. Wang, Y. Li, S. Gao, X. Yu, Y. Chen, Y. Lin, Tetrahedral framework nucleic acids can alleviate taurocholate-induced severe acute pancreatitis and its subsequent multiorgan injury in mice, Nano Lett. 22 (4) (2022) 1759–1768.
[6] S.G. Barreto, A. Habtezion, A. Gukovskaya, A. Lugea, C. Jeon, D. Yadav, P. Hegyi, V. Venglovecz, R. Sutton, S.J. Pandol, Critical thresholds: key to unlocking the door to the prevention and specific treatments for acute pancreatitis, Gut 70 (1) (2021) 194–203.
[7] M.A. Mederos, H.A. Reber, M.D. Girgis, Acute pancreatitis: a review, JAMA 325 (4) (2021) 382–390.
[8] Z. Hu, D. Wang, J. Gong, Y. Li, Z. Ma, T. Luo, X. Jia, Y. Shi, Z. Song, MSCs deliver hypoxia-treated mitochondria reprogramming acinar metabolism to alleviate severe acute pancreatitis injury, Adv. Sci. 10 (25) (2023) 2207691.
[9] J. Glaubitz, A. Wilden, F. Frost, S. Ameling, G. Homuth, H. Mazloum, M. C. Ruehlemann, C. Bang, A.A. Aghdassi, C. Budde, T. Pickartz, A. Franke, B. M. Broeker, U. Voelker, J. Mayerle, M.M. Lerch, F.U. Weiss, M. Sendler, Activated regulatory T-cells promote duodenal bacterial translocation into necrotic areas in severe acute pancreatitis, Gut 72 (7) (2023) 1355–1369.
[10] H. Li, J. Xie, X. Guo, G. Yang, B. Cai, J. Liu, M. Yue, Y. Tang, G. Wang, S. Chen, J. Guo, X. Qi, D. Wang, H. Zheng, W. Liu, H. Yu, C. Wang, S.J. Zhu, F. Guo, *Bifidobacterium spp*. and their metabolite lactate protect against acute pancreatitis *via* inhibition of pancreatic and systemic inflammatory responses, Gut Microbes 14 (1) (2022) 2127456.
[11] Y.F. Ren, M.Z. Wang, J.B. Bi, J. Zhang, L. Zhang, W.M. Liu, S.S. Wei, Y. Lv, Z. Wu, R.Q. Wu, Irisin attenuates intestinal injury, oxidative and endoplasmic reticulum stress in mice with L-arginine-induced acute pancreatitis, World J. Gastroenterol. 25 (45) (2019) 6653–6667.
[12] W.T. Kuo, L. Shen, L. Zuo, N. Shashikanth, M.L.D.M. Ong, L. Wu, J. Zha, K. L. Edelblum, Y. Wang, Y. Wang, S.P. Nilsen, J.R. Turner, Inflammation-induced Occludin downregulation limits epithelial apoptosis by suppressing Caspase-3 expression, Gastroenterology 157 (5) (2019) 1323–1337.
[13] J. Zhou, M. Li, Q. Chen, X. Li, L. Chen, Z. Dong, W. Zhu, Y. Yang, Z. Liu, Q. Chen, Programmable probiotics modulate inflammation and gut microbiota for inflammatory bowel disease treatment after effective oral delivery, Nat. Commun. 13 (1) (2022) 3432.
[14] C. Li, Z. Zhao, Y. Luo, T. Ning, P. Liu, Q. Chen, Y. Chu, Q. Guo, Y. Zhang, W. Zhou, H. Chen, Z. Zhou, Y. Wang, B. Su, H. You, T. Zhang, X. Li, H. Song, C. Li, T. Sun, C. Jiang, Macrophage-disguised manganese dioxide nanoparticles for neuroprotection by reducing oxidative stress and modulating inflammatory microenvironment in acute ischemic stroke, Adv. Sci. 8 (20) (2021) 2101526.
[15] C.W. Chou, W.T. Chia, C.H. Mac, C.Y. Wu, C.C. Chen, H.L. Song, Y.H. Lin, Y.J. Lin, H.W. Sung, Selective accumulation of ionic nanocrystal H_2 storage system as an *in situ* H_2/boric acid nanogenerator fights against ethanol-induced gastric ulcers, Chem. Eng. J. 463 (2023) 142373.
[16] E.T. Chouchani, V.R. Pell, E. Gaude, D. Aksentijević, S.Y. Sundier, E.L. Robb, A. Logan, S.M. Nadtochiy, E.N.J. Ord, A.C. Smith, F. Eyassu, R. Shirley, C.-H. Hu, A.J. Dare, A.M. James, S. Rogatti, R.C. Hartley, S. Eaton, A.S.H. Costa, P. S. Brookes, S.M. Davidson, M.R. Duchen, K.S. Parsy, M.J. Shattock, A.J. Robinson, L.M. Work, C. Frezza, T. Krieg, M.P. Murphy, Ischaemic accumulation of succinate controls reperfusion injury through mitochondrial ROS, Nature 515 (7527) (2014) 431–435.
[17] K. Zhang, J. Yang, L. Chen, J. He, D. Qu, Z. Zhang, Y. Liu, X. Li, J. Liu, J. Li, X. Xie, Q. Wang, Gut microbiota participates in polystyrene microplastics-induced hepatic injuries by modulating the gut-liver axis, ACS Nano 17 (15) (2023) 15125–15145.
[18] Y. Chen, R. Luo, J. Li, S. Wang, J. Ding, K. Zhao, B. Lu, W. Zhou, Intrinsic radical species scavenging activities of tea polyphenols nanoparticles block pyroptosis in endotoxin-induced sepsis, ACS Nano 16 (2) (2022) 2429–2441.
[19] Z. Li, Y. Feng, S. Zhang, T. Li, H. Li, D. Wang, K. Hao, C. He, H. Tian, X. Chen, A multifunctional nanoparticle mitigating cytokine storm by scavenging multiple inflammatory mediators of sepsis, ACS Nano 17 (9) (2023) 8551–8563.
[20] P. Zhang, Y. Gong, Q. Pan, Z. Fan, G. Li, M. Pei, J. Zhang, T. Wang, G. Zhou, X. Wang, W. Ren, Multifunctional calcium polyphenol networks reverse the hostile microenvironment of trauma for preventing postoperative peritoneal adhesions, Biomater. Sci. 11 (20) (2023) 6848–6861.
[21] S. Liu, Y. Cao, L. Ma, J. Sun, L. Ramos Mucci, Y. Ma, X. Yang, Z. Zhu, J. Zhang, B. Xiao, Oral antimicrobial peptide-EGCG nanomedicines for synergistic treatment of ulcerative colitis, J. Control. Release 347 (2022) 544–560.
[22] W. Lei, J. Yang, J. Wang, Z. Xiao, P. Zhou, S. Zheng, P. Zhu, Synergetic EGCG and coenzyme Q10 DSPC liposome nanoparticles protect against myocardial infarction, Biomater. Sci. 11 (20) (2023) 6862–6870.
[23] F. Liu, S. Sheng, D. Shao, Y. Xiao, Y. Zhong, J. Zhou, C.H. Quek, Y. Wang, J. Dawulieti, C. Yang, H. Tian, X. Chen, K.W. Leong, Targeting multiple mediators of sepsis using multifunctional tannic acid-Zn^{2+}-gentamicin nanoparticles, Matter 4 (11) (2021) 3677–3695.
[24] J. Ye, Q. Li, Y. Zhang, Q. Su, Z. Feng, P. Huang, C. Zhang, Y. Zhai, W. Wang, ROS scavenging and immunoregulative EGCG@Cerium complex loaded in antibacterial polyethylene glycol-chitosan hydrogel dressing for skin wound healing, Acta Biomater. 166 (2023) 155–166.
[25] A.M. Hanash, J.A. Dudakov, G. Hua, M.H. O'Connor, L.F. Young, N.V. Singer, M. L. West, R.R. Jenq, A.M. Holland, L.W. Kappel, A. Ghosh, J.J. Tsai, U.K. Rao, N. L. Yim, O.M. Smith, E. Velardi, E.B. Hawryluk, G.F. Murphy, C. Liu, L.A. Fouser, R. Kolesnick, B.R. Blazar, M.R.M. van den Brink, Interleukin-22 protects intestinal stem cells from immune-mediated tissue damage and regulates sensitivity to graft versus host disease, Immunity 37 (2) (2012) 339–350.
[26] M. Munoz, C. Eidenschenk, N. Ota, K. Wong, U. Lohmann, A.A. Kuehl, X. Wang, P. Manzanillo, Y. Li, S. Rutz, Y. Zheng, L. Diehl, N. Kayagaki, M. van Lookeren-Campagne, O. Liesenfeld, M. Heimesaat, W. Ouyang, Interleukin-22 induces interleukin-18 expression from epithelial cells during intestinal infection, Immunity 42 (2) (2015) 321–331.
[27] J. Sung, Z. Alghoul, D. Long, C. Yang, D. Merlin, Oral delivery of IL-22 mRNA-loaded lipid nanoparticles targeting the injured intestinal mucosa: a novel therapeutic solution to treat ulcerative colitis, Biomaterials 288 (2022) 121707.
[28] D.A. Garcia Topete, L.A. Aalvarez Lee, G.I. Carballo Lopez, M.A. Uriostegui Campos, C. Guzman Uribe, A.B. Castro Cesena, Antifibrotic activity of carbon quantum dots in a human *in vitro* model of non-alcoholic steatohepatitis using hepatic stellate cells, Biomater. Sci. 12 (5) (2024) 1307–1319.
[29] Z. Sun, M. Ren, B. Shan, Q. Yang, Z. Zhao, X. Liu, L. Yin, One-pot synthesis of dynamically cross-linked polymers for serum-resistant nucleic acid delivery, Biomater. Sci. 11 (16) (2023) 5653–5662.
[30] J.E. Chung, S. Tan, S.J. Gao, N. Yongvongsoontorn, S.H. Kim, J.H. Lee, H.S. Choi, H. Yano, L. Zhuo, M. Kurisawa, J.Y. Ying, Self-assembled micellar nanocomplexes comprising green tea catechin derivatives and protein drugs for cancer therapy, Nat. Nanotechnol. 9 (11) (2014) 907–912.
[31] M. Muñoz, C. Eidenschenk, N. Ota, K. Wong, U. Lohmann, A.A. Kühl, X. Wang, P. Manzanillo, Y. Li, S. Rutz, Y. Zheng, L. Diehl, N. Kayagaki, M. van Lookeren Campagne, O. Liesenfeld, M. Heimesaat, W. Ouyang, Interleukin-22 induces interleukin-18 expression from epithelial cells during intestinal infection, Immunity 42 (2) (2015) 321–331.
[32] M. Shin, H.A. Lee, M. Lee, Y. Shin, J.J. Song, S.W. Kang, D.H. Nam, E.J. Jeon, M. Cho, M. Do, S. Park, M.S. Lee, J.H. Jang, S.W. Cho, K.S. Kim, H. Lee, Targeting protein and peptide therapeutics to the heart *via* tannic acid modification, Nat. Biomed. Eng. 2 (5) (2018) 304–317.
[33] G. Rong, L. Chen, F. Zhu, E. Tan, Y. Cheng, Polycatechols with robust efficiency in cytosolic peptide delivery *via* catechol-boronate chemistry, Nano Lett. 22 (15) (2022) 6245–6253.
[34] X. Liu, Z. Zhao, W. Li, Y. Li, Q. Yang, N. Liu, Y. Chen, L. Yin, Engineering nucleotidoproteins for base-pairing-assisted cytosolic delivery and genome editing, Angew. Chem. Int. Ed. 62 (45) (2023) e2023076.
[35] P. Liu, T. Zhang, Q. Chen, C. Li, Y. Chu, Q. Guo, Y. Zhang, W. Zhou, H. Chen, Z. Zhou, Y. Wang, Z. Zhao, Y. Luo, X. Li, H. Song, B. Su, C. Li, T. Sun, C. Jiang, Biomimetic dendrimer-peptide conjugates for early multi-target therapy of Alzheimer's disease by inflammatory microenvironment modulation, Adv. Mater. 33 (26) (2021) 2100746.
[36] K. Wang, Q. Chen, L. Ding, Y. Zhu, X. Wang, M. Zhou, M. Chang, M. Pei, Y. Zhang, Y. Zhang, Y. Chen, H. Qin, Mucoadhesive probiotic-based oral microcarriers with prolonged intestinal retention for inflammatory bowel disease therapy, Nano Today 50 (2023) 101876.
[37] N.G. Kotla, I.L.M. Isa, S. Rasala, S. Demir, R. Singh, B.V. Baby, S.K. Swamy, P. Dockery, V.R. Jala, Y. Rochev, A. Pandit, Modulation of gut barrier functions in ulcerative colitis by hyaluronic acid system, Adv. Sci. 9 (4) (2022) 2103189.
[38] C. Zhao, Z. Li, J. Chen, L. Su, J. Wang, D.S. Chen, J. Ye, N. Liao, H. Yang, J. Song, J. Shi, Site-specific biomimicry of antioxidative melanin formation and its application for acute liver injury therapy and imaging, Adv. Mater. 33 (34) (2021) 2102391.
[39] W. Lin, K. Hu, C. Li, W. Pu, X. Yan, H. Chen, H. Hu, H. Deng, J. Zhang, A multi-bioactive nanomicelle-based "one stone for multiple birds" strategy for precision therapy of abdominal aortic aneurysms, Adv. Mater. 34 (44) (2022) 2204455.
[40] J. Tan, Z. Deng, G. Liu, J. Hu, S. Liu, Anti-inflammatory polymersomes of redox-responsive polyprodrug amphiphiles with inflammation-triggered indomethacin release characteristics, Biomaterials 178 (2018) 608–619.
[41] Z. Zhao, X. Liu, M. Hou, R. Zhou, F. Wu, J. Yan, W. Li, Y. Zheng, Q. Zhong, Y. Chen, L. Yin, Endocytosis-independent and cancer-selective cytosolic protein delivery *via* reversible tagging with LAT1 substrate, Adv. Mater. 34 (35) (2022) 2110560.
[42] X. Gao, C. Yuan, E. Tan, Z. Li, Y. Cheng, J. Xiao, G. Rong, Dual-responsive bioconjugates bearing a bifunctional adaptor for robust cytosolic peptide delivery, J. Control. Release 355 (2023) 675–684.
[43] L. Shao, S. Oshima, B. Duong, R. Advincula, J. Barrera, B.A. Malynn, A. Ma, A20 restricts Wnt signaling in intestinal epithelial cells and suppresses colon carcinogenesis, PLoS One 8 (5) (2013) e62223.
[44] J. Gout, R.M. Pommier, D.F. Vincent, B. Kaniewski, S. Martel, U. Valcourt, L. Bartholin, Isolation and culture of mouse primary pancreatic acinar cells, J. Vis. Exp. 78 (2013) e50514.
[45] X. Zhang, Y. Chen, H. He, S. Wang, Z. Lei, F. Zhang, ROS/RNS and base dual activatable merocyanine-based NIR-II fluorescent molecular probe for *in vivo* biosensing, Angew. Chem. Int. Ed. 60 (50) (2021) 26337–26341.
[46] R. Re, N. Pellegrini, A. Proteggente, A. Pannala, M. Yang, C. Rice-Evans, Antioxidant activity applying an improved ABTS radical cation decolorization assay, Free Radic. Biol. Med. 26 (9–10) (1999) 1231–1237.
[47] S. Zhu, B. Liu, F. Wang, D. Huang, F. Zhong, Y. Li, Characterization and *in vitro* digestion properties of cassava starch and epigallocatechin-3-gallate (EGCG) blend, LWT 137 (2021) 110398.
[48] G. Perides, G.J.D. van Acker, J.M. Laukkarinen, M.L. Steer, Experimental acute biliary pancreatitis induced by retrograde infusion of bile acids into the mouse pancreatic duct, Nat. Protoc. 5 (2) (2010) 335–341.

[49] A. Chaitoff, A.S. Cifu, J.D. Niforatos, Initial management of acute pancreatitis, JAMA 323 (22) (2020) 2331–2332.
[50] O.J. Bakker, S. van Brunschot, H.C. van Santvoort, M.G. Besselink, T.L. Bollen, M. A. Boermeester, C.H. Dejong, H. van Goor, K. Bosscha, U. Ahmed Ali, S. Bouwense, W.M. van Grevenstein, J. Heisterkamp, A.P. Houdijk, J.M. Jansen, T.M. Karsten, E. R. Manusama, V.B. Nieuwenhuijs, A.F. Schaapherder, G.P. van der Schelling, M. P. Schwartz, B.W. Spanier, A. Tan, J. Vecht, B.L. Weusten, B.J. Witteman, L. M. Akkermans, M.J. Bruno, M.G. Dijkgraaf, B. van Ramshorst, H.G. Gooszen, G. Dutch, Pancreatitis study, early versus on-demand nasoenteric tube feeding in acute pancreatitis, N. Engl. J. Med. 371 (21) (2014) 1983–1993.
[51] Y. Lee, K. Sugihara, M.G. Gillilland III, S. Jon, N. Kamada, J.J. Moon, Hyaluronic acid-bilirubin nanomedicine for targeted modulation of dysregulated intestinal barrier, microbiome and immune responses in colitis, Nat. Mater. 19 (1) (2020) 118.
[52] J. Schmidt, D.W. Rattner, K. Lewandrowski, C.C. Compton, U. Mandavilli, W. T. Knoefel, A.L. Warshaw, A better model of acute-pancreatitis for evaluating therapy, Ann. Surg. 215 (1) (1992) 44–56.
[53] Y. Wei, X. Li, J. Lin, Y. Zhou, J. Yang, M. Hou, F. Wu, J. Yan, C. Ge, D. Hu, L. Yin, Oral delivery of siRNA using fluorinated, small-sized nanocapsules toward anti-inflammation treatment, Adv. Mater. 35 (11) (2023) 2206821.
[54] W. Yang, T. Yu, X. Huang, A.J. Bilotta, L. Xu, Y. Lu, J. Sun, F. Pan, J. Zhou, W. Zhang, S. Yao, C.L. Maynard, N. Singh, S.M. Dann, Z. Liu, Y. Cong, Intestinal microbiota-derived short-chain fatty acids regulation of immune cell IL-22 production and gut immunity, Nat. Commun. 11 (1) (2020) 4457.
[55] X. Xie, J. Zhao, W. Gao, J. Chen, B. Hu, X. Cai, Y. Zheng, Prussian blue nanozyme-mediated nanoscavenger ameliorates acute pancreatitis *via* inhibiting TLRs/NF-κB signaling pathway, Theranostics 11 (7) (2021) 3213–3228.
[56] L. Zhang, P. Xie, H. Wu, J. Zhao, S. Wang, 2D $MoSe_2$@PVP nanosheets with multi-enzyme activity alleviate the acute pancreatitis *via* scavenging the reactive oxygen and nitrogen species, Chem. Eng. J. 446 (2022) 136792.
[57] L. Liu, W. Wu, S. Li, L. Ma, Y. Liu, X. Wang, Y. Jiang, Engineered baicalein-decorated zinc phosphates for synergistic alleviation of inflammatory bowel disease by repairing the mucosal barrier and relieving oxidative stress, Biomater. Sci. 11 (23) (2023) 7678–7691.
[58] N. Singh, V. Ahuja, V. Sachdev, A.D. Upadhyay, R. Goswami, L. Ramakrishnan, S. Dwivedi, A. Saraya, Antioxidants for pancreatic functions in chronic pancreatitis: a double-blind randomized placebo-controlled pilot study, J. Clin. Gastroenterol. 54 (3) (2020) 284–293.
[59] X. Jiang, Y.W. Zheng, S. Bao, H. Zhang, R. Chen, Q. Yao, L. Kou, Drug discovery and formulation development for acute pancreatitis, Drug Deliv. 27 (1) (2020) 1562–1580.
[60] Y. Wang, D. Qian, X. Wang, X. Zhang, Z. Li, X. Meng, L. Yu, X. Yan, Z. He, Biomimetic trypsin-responsive structure-bridged mesoporous organosilica nanomedicine for precise treatment of acute pancreatitis, ACS Nano 18 (29) (2024) 19283–19302.